Elastic Coiling-up-Space Metamaterial

Geun Ju Jeon and Joo Hwan Oh*

Department of Mechanical Engineering, Ulsan National Institute of Science and Technology, UNIST-gil 50, Eonyang-eup, Ulju-gun, Ulsan, 44919, Korea

(Received 29 June 2021; revised 16 November 2021; accepted 18 November 2021; published 6 December 2021)

Coiling up space is a metamaterial technique that utilizes a subwavelength labyrinthine structure to achieve a high refractive index. Despite the various advances in acoustics, the coiling-up-space technique cannot be used in the elastic case owing to its tensor-based physics. In this study, we show that an elastic coiling up space is possible if the "fluidlike connection" and "isocurvature path" conditions are satisfied. These conditions overcome the tensorial nature of elastic waves and allow the change of displacement fields according to the geometry, as in the acoustic case with scalar fields. The proposed elastic coiling-up-space technique is numerically and experimentally demonstrated.

DOI: 10.1103/PhysRevApplied.16.064016

I. INTRODUCTION

Coiling up space is a branch of acoustic metamaterials that utilizes a subwavelength labyrinthine structure to achieve unusual acoustic phenomena. Unlike the most general approach that relies on locally resonating subwavelength structures, acoustic metamaterials with a coiling up space utilize a high refractive index from the labyrinthine structure. Because an acoustic wave is a scalar field, waves inside the labyrinthine structure would propagate along the mazelike wave path, as shown in Fig. 1(a). Therefore, the labyrinthine structure acts as an acoustic medium with an extremely high refractive index, which can be easily controlled by the degree of coiling. Owing to these characteristics, the idea of coiling up space has enabled various advances in metamaterials and metasurfaces since it was proposed by Liang *et al*. [1], such as achieving density near zero [1], negative index [1–3], acoustic focusing [4–8], extraordinary transmission [9], sound absorption [10–14], and extremely slow waves [15]. Furthermore, it has contributed to the miniaturization of acoustic metamaterials and metasurfaces [16,17].

Despite the various advances of coiling up space in metamaterials and metasurfaces, they have been limited to acoustic cases only. In acoustics, as mentioned earlier, waves are governed by a scalar field so that waves can propagate freely inside the labyrinthine structure as if the structure has a straight configuration. However, if waves are not governed by a scalar field, waves inside the labyrinthine structure cannot propagate freely as they do in free space. In fact, there have been several attempts to apply coiling up spaces in electromagnetic metamaterials, such as double-negative-index media [18], but these studies showed that the band structure of the electromagnetic coiling up space was largely different from the acoustic version. Unlike the acoustic case, where band folding clearly occurs without band gaps, coiled-up electromagnetic metamaterials exhibit band-gap and dispersive wave phenomena. Owing to this issue, the conventional spiral structure has been extensively used to achieve a high refractive index for electromagnetic waves, instead of the coiling-up-space technique [19].

The aforementioned issue becomes more severe in the elastic case, whereby waves are governed by tensor fields. Figure 1(b) plots the elastic wave propagating inside a typical labyrinthine structure. For the acoustic case shown in Fig. 1(a), the wave-front plot shows that acoustic waves are guided well along the labyrinthine structure. However, for the elastic case shown in Fig. 1(b), the wave propagating direction is not guided at all, and the direction does not significantly change regardless of the labyrinthine structure. Moreover, the wave-front plot in Fig. 1(b) shows that each segment of the labyrinthine structure exhibits different deformations, thus indicating that mode conversion is actively taking place. Thus, the band structure shows a large band gap, as shown in Fig. 1(b), unlike the acoustic case, which shows clear band folding without band gaps, as shown in Fig. 1(a). In addition, the refractive index is not dominated by the degree of coiling. Owing to this physical difference, the elastic coiling up space has never been studied or realized thus far.

One may consider the previous research on "fluidlike elastic metamaterials" [20,21] as a solution for this issue. Unfortunately, in elastic coiling up space, we find that the previous research cannot be applied at all. Since we are focusing on the longitudinal wave, the shear modulus has nothing to do with the current problem. Furthermore, we find that "eliminating all stiffnesses other than the

*joohwan.oh@unist.ac.kr

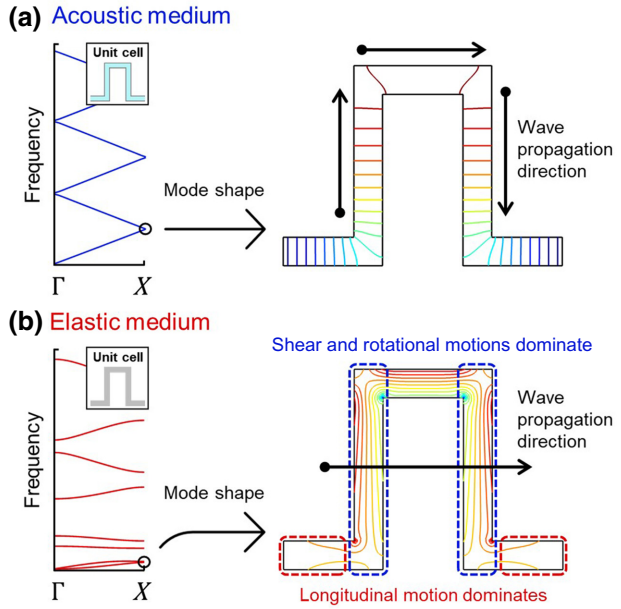

FIG. 1. Band structure and mode shape of the labyrinthine structure for (a) acoustic medium and (b) elastic medium.

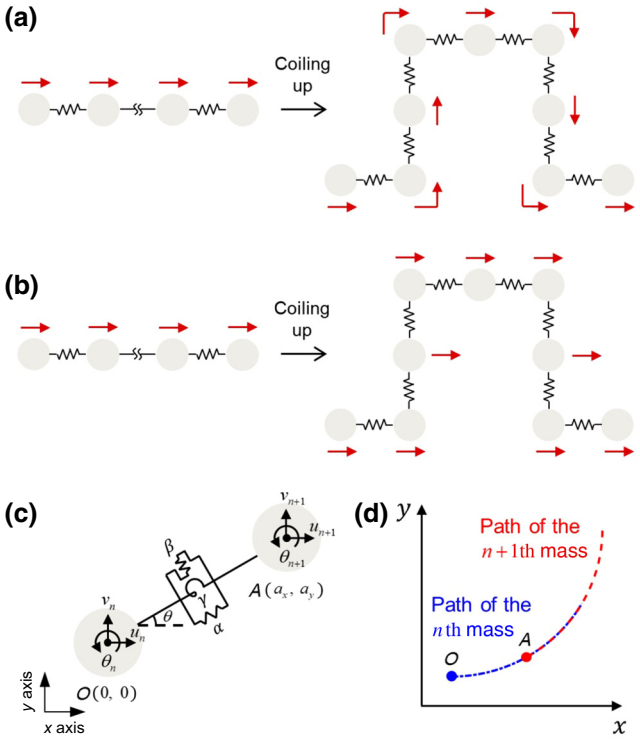

FIG. 2. General periodic mass-spring chain and its coiled-up structure for (a) acoustic case and (b) elastic case. (c) Two masses connected by three types of springs, namely a translational spring, shear spring, and a rotational spring, each with spring coefficients α, β, γ. (d) Numerically calculated possible path of motion of the two masses that enables the change of displacement fields (the blue and red dotted lines indicate the path of motion of the n^{th} and the $n+1^{\text{th}}$ masses, respectively).

longitudinal one" is not enough to achieve elastic coiling up space, as shown in Sec. III A. In fact, "achieving elastic coiling up space" is a totally different problem from "achieving fluidlike elastic metamaterials," in that the physical requirements for each case are totally different. Achieving elastic coiling up space, including the requirements and actual realization, has never yet been presented.

Herein, we present a method to achieve an elastic coiling up space with actual realization. As explained, if the labyrinthine structure is applied without any specific conditions, the elastic wave does not change its propagating direction, and mode coupling actively takes place. Thus, if we determine the specific conditions that allow elastic waves to change their propagating direction without mode coupling, we can overcome the limitation of tensor fields; elastic coiling up space thus becomes possible. From theoretical investigations, we determine two specific conditions that enable an elastic coiling up space. Based on the specific conditions, we design, simulate, fabricate, and realize an elastic coiling up space.

II. BACKGROUND THEORY

A. Specific conditions for elastic coiling up space

First, we aim to derive specific conditions for the elastic coiling up space. To obtain an idea, a general periodic mass-spring chain and its coiled-up structure are considered, as shown in Fig. 2. Because the elastic coiling up space mainly deals with low frequencies below the homogenization limit, we ignore the inertial effect, which simplifies our approach and allows us to focus on the zero-frequency rigid-body motion. In the acoustic case, waves are governed by a scalar field so that their propagating directions are defined by the configuration of the structure, as shown in Fig. 2(a). Conversely, in the elastic case where tensor fields dominate waves, the rigid-body motion in Fig. 2(b) is largely different from the acoustic case. The dominant displacement is not affected by the geometric change, thus indicating that mode conversion actively takes place, and the propagation direction of the wave is not altered by the coiling up space. Herein, we postulate a reasonable assumption that if we achieve acoustic rigid-body motion as in Fig. 2(a) in the elastic regime with several specific conditions, elastic coiling up space is enabled. Based on this assumption, a theoretical investigation is presented. In addition, we show that the derived conditions also work when the inertial effects are not ignored.

Because now we are focusing on the rigid-body motion that excludes any deformation of the body, there is no interactive force between each mass so we can disassemble several masses in coiled-up structures, as shown in

Fig. 2(b). As shown in Fig. 2(c), two masses are disassembled. Three types of springs, namely, the translational spring, shear spring, and rotational spring, with spring coefficients α, β, and γ, are considered to mimic longitudinal, shear, and rotational deformations in elastic media, respectively. Accordingly, two inertial terms, mass m and rotational inertia I, are considered for each mass. $O(0,\ 0)$ and $A(a_x,\ a_y)$ are the initial positions of the masses. $(u_n,\ v_n,\ \theta_n)$ and $(u_{n+1},\ v_{n+1},\ \theta_{n+1})$ are the x- and y-directional displacements, and the angle of rotation of the masses. To consider the geometric change in the coiling up space, θ and $\Delta\theta$ are introduced, where θ is the angle between the line connecting the two masses and the x axis, and $\Delta\theta$ is the change in the angle owing to the motion of each mass. Considering that there are no external forces or moments for the rigid-body motion, the equation of motion for each mass can be expressed as follows:

$$m\frac{\partial^2 u_n}{\partial t^2} = [\alpha\cos(\theta+\Delta\theta)+\beta\sin(\theta+\Delta\theta)]\left(\sqrt{(a_x+u_{n+1}-u_n)^2+(a_y+v_{n+1}-v_n)^2}-\sqrt{a_x^2+a_y^2}\right) + \frac{\gamma(\theta_{n+1}-\theta_n-\Delta\theta)\sin(\theta+\Delta\theta)}{\sqrt{(a_x+u_{n+1}-u_n)^2+(a_y+v_{n+1}-v_n)^2}}, \tag{1a}$$

$$m\frac{\partial^2 u_{n+1}}{\partial t^2} = [\alpha\cos(\theta+\Delta\theta)+\beta\sin(\theta+\Delta\theta)]\left(\sqrt{a_x^2+a_y^2}-\sqrt{(a_x+u_{n+1}-u_n)^2+(a_y+v_{n+1}-v_n)^2}\right) + \frac{\gamma(\theta_{n+1}-\theta_n+\Delta\theta)\sin(\theta+\Delta\theta)}{\sqrt{(a_x+u_{n+1}-u_n)^2+(a_y+v_{n+1}-v_n)^2}}, \tag{1b}$$

$$m\frac{\partial^2 v_n}{\partial t^2} = [\alpha\sin(\theta+\Delta\theta)+\beta\cos(\theta+\Delta\theta)]\left(\sqrt{(a_x+u_{n+1}-u_n)^2+(a_y+v_{n+1}-v_n)^2}-\sqrt{a_x^2+a_y^2}\right) + \frac{\gamma(\theta_n-\theta_{n+1}+\Delta\theta)\cos(\theta+\Delta\theta)}{\sqrt{(a_x+u_{n+1}-u_n)^2+(a_y+v_{n+1}-v_n)^2}}, \tag{1c}$$

$$m\frac{\partial^2 v_{n+1}}{\partial t^2} = [\alpha\sin(\theta+\Delta\theta)+\beta\cos(\theta+\Delta\theta)]\left(\sqrt{a_x^2+a_y^2}-\sqrt{(a_x+u_{n+1}-u_n)^2+(a_y+v_{n+1}-v_n)^2}\right) + \frac{\gamma(\theta_n-\theta_{n+1}-\Delta\theta)\cos(\theta+\Delta\theta)}{\sqrt{(a_x+u_{n+1}-u_n)^2+(a_y+v_{n+1}-v_n)^2}}, \tag{1d}$$

$$I\frac{\partial^2\theta_n}{\partial t^2} = \gamma(\theta_{n+1}-\theta_n+\Delta\theta), \tag{1e}$$

$$I\frac{\partial^2\theta_{n+1}}{\partial t^2} = \gamma(\theta_n-\theta_{n+1}+\Delta\theta). \tag{1f}$$

Assuming rigid-body motion, the inertial terms become zero; hence, Eq. (1) can be rewritten as follows:

$$[\alpha\cos(\theta+\Delta\theta)+\beta\sin(\theta+\Delta\theta)]\left(\sqrt{(a_x+u_{n+1}-u_n)^2+(a_y+v_{n+1}-v_n)^2}-\sqrt{a_x^2+a_y^2}\right) + \frac{\gamma(\theta_{n+1}-\theta_n-\Delta\theta)\sin(\theta+\Delta\theta)}{\sqrt{(a_x+u_{n+1}-u_n)^2+(a_y+v_{n+1}-v_n)^2}} = 0, \tag{2a}$$

$$[\alpha\cos(\theta+\Delta\theta)+\beta\sin(\theta+\Delta\theta)]\left(\sqrt{a_x^2+a_y^2}-\sqrt{(a_x+u_{n+1}-u_n)^2+(a_y+v_{n+1}-v_n)^2}\right) + \frac{\gamma(\theta_{n+1}-\theta_n+\Delta\theta)\sin(\theta+\Delta\theta)}{\sqrt{(a_x+u_{n+1}-u_n)^2+(a_y+v_{n+1}-v_n)^2}} = 0, \tag{2b}$$

$$[\alpha\sin(\theta+\Delta\theta)+\beta\cos(\theta+\Delta\theta)]\left(\sqrt{(a_x+u_{n+1}-u_n)^2+(a_y+v_{n+1}-v_n)^2}-\sqrt{a_x^2+a_y^2}\right)$$
$$+\frac{\gamma(\theta_n-\theta_{n+1}+\Delta\theta)\cos(\theta+\Delta\theta)}{\sqrt{(a_x+u_{n+1}-u_n)^2+(a_y+v_{n+1}-v_n)^2}}=0, \tag{2c}$$

$$[\alpha\sin(\theta+\Delta\theta)+\beta\cos(\theta+\Delta\theta)]\left(\sqrt{a_x^2+a_y^2}-\sqrt{(a_x+u_{n+1}-u_n)^2+(a_y+v_{n+1}-v_n)^2}\right)$$
$$+\frac{\gamma(\theta_n-\theta_{n+1}-\Delta\theta)\cos(\theta+\Delta\theta)}{\sqrt{(a_x+u_{n+1}-u_n)^2+(a_y+v_{n+1}-v_n)^2}}=0, \tag{2d}$$

$$\gamma(\theta_{n+1}-\theta_n+\Delta\theta)=0, \tag{2e}$$

$$\gamma(\theta_n-\theta_{n+1}+\Delta\theta)=0. \tag{2f}$$

First, consider Eqs. (2e) and (2f). Adding Eqs. (2e) and (2f) yields

$$\gamma\Delta\theta=0. \tag{3}$$

For the solution of Eq. (3), the following two solution forms can be considered,

$$\gamma=0, \tag{4a}$$

or

$$\Delta\theta=0. \tag{4b}$$

However, Eq. (4b) is a trivial solution because it is only valid when there is no rotational motion, that is, the structure has a straight configuration. Thus, Eq. (4a) is the only available solution. This means that zero rotational stiffness should be introduced for the desired rigid-body motion. Now, let us consider Eqs. (2a)–(2d). Substituting Eq. (4a) in Eq. (2) yields the following equations:

$$0=[\alpha\cos(\theta+\Delta\theta)+\beta\sin(\theta+\Delta\theta)]\left(\sqrt{(a_x+u_{n+1}-u_n)^2+(a_y+v_{n+1}-v_n)^2}-\sqrt{a_x^2+a_y^2}\right), \tag{5a}$$

$$0=[\alpha\cos(\theta+\Delta\theta)+\beta\sin(\theta+\Delta\theta)]\left(\sqrt{a_x^2+a_y^2}-\sqrt{(a_x+u_{n+1}-u_n)^2+(a_y+v_{n+1}-v_n)^2}\right), \tag{5b}$$

$$0=[\alpha\sin(\theta+\Delta\theta)+\beta\cos(\theta+\Delta\theta)]\left(\sqrt{(a_x+u_{n+1}-u_n)^2+(a_y+v_{n+1}-v_n)^2}-\sqrt{a_x^2+a_y^2}\right), \tag{5c}$$

$$0=[\alpha\sin(\theta+\Delta\theta)+\beta\cos(\theta+\Delta\theta)]\left(\sqrt{a_x^2+a_y^2}-\sqrt{(a_x+u_{n+1}-u_n)^2+(a_y+v_{n+1}-v_n)^2}\right). \tag{5d}$$

For the solution of Eq. (5), the following two solution forms can be considered.

$$\alpha=\beta=0, \tag{6a}$$

or

$$\sqrt{(a_x+u_{n+1}-u_n)^2+(a_y+v_{n+1}-v_n)^2}-\sqrt{a_x^2+a_y^2}=0. \tag{6b}$$

However, Eq. (6a) indicates that the two masses are disconnected, which is a trivial solution. Thus, Eq. (6b) is the only available solution. Squaring both sides of Eq. (6b) yields

$$2a_x(u_{n+1}-u_n)+(u_{n+1}-u_n)^2 + 2a_y(v_{n+1}-v_n)+(v_{n+1}-v_n)^2=0. \tag{7}$$

In the coiling up space, there should be no internal reflection. In other words, the magnitude of the displacement vectors for both masses should be the same and can be expressed as

$$\sqrt{(u_{n+1})^2+(v_{n+1})^2}=\sqrt{(u_n)^2+(v_n)^2}. \tag{8}$$

Equation (8) can be rearranged with respect to v_{n+1} as follows:

$$v_{n+1}=\sqrt{(u_n)^2+(v_n)^2-(u_{n+1})^2}. \tag{9}$$

Substituting Eq. (9) into Eq. (7) yields the following:

$$2a_x(u_{n+1}-u_n)+(u_{n+1}-u_n)^2+2a_y \times\left(\sqrt{(u_n)^2+(v_n)^2-(u_{n+1})^2}-v_n\right) +\left(\sqrt{(u_n)^2+(v_n)^2-(u_{n+1})^2}-v_n\right)^2=0. \tag{10}$$

The solutions for u_{n+1} in Eq. (10) can be written as follows:

$$u_{n+1}=u_n, \tag{11a}$$

or

$$u_{n+1}=[u_n\{(a_x-u_n)^2-(a_y^2-v_n^2)\}+2v_na_x(a_y-v_n)]/ [(a_x-u_n)^2+(a_y-v_n)^2]. \tag{11b}$$

The solutions for v_{n+1} in Eq. (10) can be written as follows:

$$v_{n+1}=v_n, \tag{12a}$$

or

$$v_{n+1}=[v_n\{(a_y-v_n)^2-(a_x^2-u_n^2)\}+2u_na_y(a_x-u_n)]/ [(a_x-u_n)^2+(a_y-v_n)^2]. \tag{12b}$$

However, Eqs. (11a) and (12a) indicate that the two masses move along the same direction; these solutions are trivial solutions. Thus, Eqs. (11b) and (12b) are the only available solutions that enable the change of displacement fields according to the geometry. Consequently, the specific conditions for the elastic coiling up space are derived as follows:

$$\gamma=0, \tag{13a}$$

$$u_{n+1}=[u_n\{(a_x-u_n)^2-(a_y^2-v_n^2)\}+2v_na_x(a_y-v_n)]/ [(a_x-u_n)^2+(a_y-v_n)^2], \tag{13b}$$

$$v_{n+1}=[v_n\{(a_y-v_n)^2-(a_x^2-u_n^2)\}+2u_na_y(a_x-u_n)]/ [(a_x-u_n)^2+(a_y-v_n)^2]. \tag{13c}$$

Equation (13a) indicates that each mass has fluidlike connections with neighboring masses—only longitudinal forces can be transferred between each mass. Equations (13b) and (13c) appear complicated; hence, we numerically plot the possible moving path of the mass n and $n+1$ for nonzero θ in Fig. 2(d). From Fig. 2(d), it can be observed that this rigid-body motion means that all masses move along a circular path with a constant curvature. Obviously, this is what we desire because the displacement fields are tangential to the circular path, as shown in Fig. 2(a).

Although the desired rigid-body motion is attained, it cannot be easily utilized because various other rigid-body motions also exist, making it almost impossible to utilize the motion. However, with specific conditions that restrict the motion of each mass, the desired rigid-body motion can be utilized effectively. The specific conditions that utilize the desired rigid-body motion and allow the elastic coiling up space are summarized as follows:

(i) Fluidlike connection: very small rotational stiffness compared with other stiffnesses ($\gamma \ll \alpha,\ \beta$)
(ii) Isocurvature path: masses only move along a circular path with constant curvature

B. Theoretical validation of specific conditions in dynamic cases

The aforementioned conditions are derived from a static case with rigid-body motions. Thus, it is essential to check whether these conditions are also valid for dynamic cases. To address this issue, the mass-spring chain under the aforementioned specific conditions is investigated analytically without neglecting the inertial terms. First, as a comparison group, a one-dimensional mass-spring chain shown in Fig. 3(a) is investigated. Each mass has the same mass m connected to a spring with coefficient α, where Δx is the distance between the masses. The force equilibrium equation for the nth mass of the one-dimensional

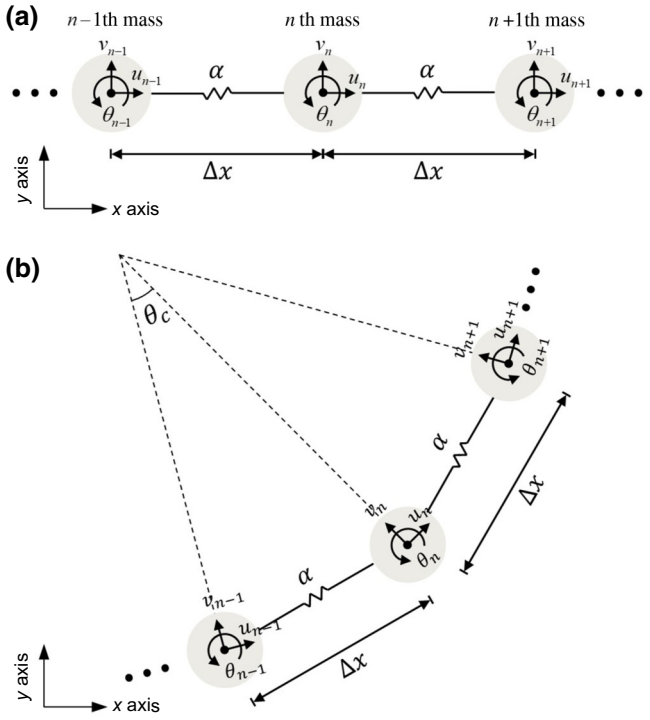

FIG. 3. (a) Mass-spring system for one-dimensional translational motion, (b) mass-spring system under the specific conditions of fluidlike connection and isocurvature path.

mass-spring chain shown in Fig. 3(a) yields

$$m\frac{\partial^2 u_n}{\partial t^2} = \alpha(u_{n+1} - 2u_n + u_{n-1}). \tag{14}$$

Multiplying the right-hand side of Eq. (14) by $(\Delta x)^2/(\Delta x)^2$ yields

$$m\frac{\partial^2 u_n}{\partial t^2} = \alpha(\Delta x)^2\frac{u_{n+1} - 2u_n + u_{n-1}}{(\Delta x)^2}. \tag{15}$$

At the frequency below the homogenization limit, the following finite difference formula is used:

$$\frac{\partial^2 u_n}{\partial x^2} = \frac{u_{n+1} - 2u_n + u_{n-1}}{(\Delta x)^2}. \tag{16}$$

Substituting the assumption in Eq. (15) yields

$$\frac{\partial^2 u_n}{\partial t^2} = \frac{\alpha(\Delta x)^2}{m}\frac{\partial^2 u_n}{\partial x^2}. \tag{17}$$

In this study, the longitudinal wave is mainly considered. Assuming the longitudinal wave and using the relationship between Young's modulus and spring coefficient to be $\alpha = EA/\Delta x$ and the relationship between mass and density to be $m = \rho A\Delta x$, where E, ρ, and A denote the Young's modulus, density, and cross-section area, respectively, Eq. (17) can be simplified as

$$\frac{\partial^2 u_n}{\partial t^2} = \frac{E}{\rho}\frac{\partial^2 u_n}{\partial x^2}. \tag{18}$$

Equation (18) can also be expressed as

$$\frac{\partial^2 u_n}{\partial t^2} = c_1^2\frac{\partial^2 u_n}{\partial x^2},\ c_1 = \sqrt{\frac{E}{\rho}}. \tag{19}$$

Equation (19) is the same as the wave equation for a one-dimensional, longitudinal elastic wave.

Subsequently, the mass-spring chain in which the direction of the displacement field changes is investigated under the specific conditions of fluidlike connection and isocurvature path, as shown in Fig. 3(b). Because the mass-spring chain operates according to the fluidlike connection condition, only a translational spring is considered. As in the previous section, (u_n, v_n, θ_n) represents the horizontal and vertical displacements with respect to the circular path and the angle of rotation of the nth mass. Additionally, Δx is the distance between each mass, and θ_c is the central angle between the lines connecting the center of the circle and each mass, as shown in Fig. 3(b). The force equilibrium equation for the nth mass of the one-dimensional mass-spring chain shown in Fig. 3(b) yields

$$m\frac{\partial^2 u_n}{\partial t^2} = \alpha\left(u_{n+1}\cos\frac{\theta_c}{2} - u_n\cos\frac{\theta_c}{2}\right)\cos\frac{\theta_c}{2} + \alpha \times \left(u_{n-1}\cos\frac{\theta_c}{2} - u_n\cos\frac{\theta_c}{2}\right)\cos\frac{\theta_c}{2} \tag{20}$$

$$= \alpha\left(\cos\frac{\theta_c}{2}\right)^2(u_{n+1} - 2u_n + u_{n-1}). \tag{21}$$

Multiplying the right-hand side of Eq. (20) by $(\Delta x)^2/(\Delta x)^2$ yields

$$m\frac{\partial^2 u_n}{\partial t^2} = \alpha\left(\cos\frac{\theta_c}{2}\right)^2(\Delta x)^2\frac{(u_{n+1} - 2u_n + u_{n-1})}{(\Delta x)^2}. \tag{22}$$

Using the finite difference formula of the second derivatives, as expressed in Eq. (16), Eq. (21) can be approximated as

$$\frac{\partial^2 u_n}{\partial t^2} = \frac{\alpha(\Delta x)^2}{m}\left(\cos\frac{\theta_c}{2}\right)^2\frac{\partial^2 u_n}{\partial x^2}. \tag{23}$$

Using the relationship between Young's modulus and the spring coefficient, i.e., $\alpha = EA/\Delta x$, and the relationship

between mass and density as $m = \rho A \Delta x$, Eq. (22) can be simplified to

$$\frac{\partial^2 u_n}{\partial t^2} = \frac{E}{\rho}\left(\cos\frac{\theta_c}{2}\right)^2 \frac{\partial^2 u_n}{\partial x^2}. \tag{24}$$

Equation (23) can also be expressed as

$$\frac{\partial^2 u_n}{\partial t^2} = c_2^2 \frac{\partial^2 u_n}{\partial x^2},\ c_2 = \sqrt{\frac{E}{\rho}}\cos\frac{\theta_c}{2}. \tag{25}$$

Comparing Eq. (24) with Eq. (19), it can be observed that the two equations are the same if the wave speed is slightly reduced from c_1 to c_2. This indicates that although the structure is curved, the wave inside the structure is the same as the longitudinal wave inside a straight bar with a slightly slower wave speed. This is what we intend to achieve—the wave can propagate unhindered despite the geometric change. Therefore, the aforementioned conditions are still valid, not only at zero frequency but also at frequencies below the homogenization limit for the elastic coiling up space.

III. ELASTIC COILING-UP-SPACE METAMATERIAL

From the theoretical approach, we conclude that fluidlike connection and isocurvature path are required to realize the concept of elastic coiling up space. Based on these specific conditions, we design an elastic coiling-up-space metamaterial. First, to achieve the fluidlike connection, we need a structure whose longitudinal stiffness is substantially larger than its rotational stiffness. To this end, we adapt a well-known bow-tie-shaped configuration [22]. Because its thinnest region is at its middle, it has a very small rotational stiffness compared with its longitudinal stiffness (please see the detailed information in Appendix A). In addition, to satisfy the isocurvature path condition, we consider the curvilinear rail and slider on which all masses are placed. Unlike the theoretical mass-spring system, all masses have a nonzero size. Thus, in the metamaterial design, only the centers of all the masses are connected to the rail. In other words, the center of each mass can only move along the predefined path of the curvilinear rail so that all masses can rotate and move along the path. Figure 4(a) shows the actual design of our elastic coiling-up-space metamaterial. Note that there exist several singular points wherein the sign of curvature changes because a full isocurvature path forms a closed circular loop so that it cannot be used to form a unit cell of metamaterial.

A. Numerical validation of the elastic coiling-up-space metamaterial

Based on the unit cell shown in Fig. 4(a), numerical investigations are performed. To determine whether elastic coiling up space is possible with our metamaterial, the band structure is numerically calculated. If the unit cell enables elastic coiling up space, there is no significant band gap and band folding can be clearly observed in the band structure, as shown in Fig. 1(a). The commercial program COMSOL Multiphysics is used to calculate the band structure. After modeling the continuum part of the unit cell shown in Fig. 4(a), appropriate roller conditions are applied for the center point of each mass to mimic the condition in which all masses are placed on the curvilinear rail. Finally, the conventional approach for the calculation of the eigenfrequencies under the proper Floquet-Bloch condition is used. Figure 4(b) shows the calculated band structure. Focusing on the longitudinal wave mode, clear band folding can be observed with almost negligible band gaps at $k = 0$ and π/d. Because each mass can also have rotational motion, there also exists an undesired rotational wave mode, as shown in Fig. 4(b). However, in Fig. 4(b), it can be clearly observed that the branches for the longitudinal and rotational modes have various intersections. This indicates that there is no mode coupling in the proposed metamaterial so that the rotational mode does not affect the longitudinal mode. These two findings, the band structure configuration and fully decoupled wave modes, strongly validate the fact that elastic coiling up space is achieved by our metamaterial design.

For further validation, we introduce two metamaterials with the same unit cell size, as shown in Figs. 4(c) and 4(d). The first is a simple continuum structure that disobeys the specific conditions proposed in this study. The other satisfies the fluidlike connection, but the masses are placed on an angled path so that the isocurvature path condition is disobeyed. For each metamaterial, the band structure is calculated as shown in Figs. 4(c) and 4(d). Compared with the elastic coiling-up-space case in Fig. 4(b), various band gaps are observed. In addition, in Fig. 4(d), it can be observed that band gaps are formed in regions in which the two branches seem to intersect with each other. This indicates that mode coupling exists despite the fluidlike condition. These results show that both conditions, namely, fluidlike connection and isocurvature path, are essential to achieve the elastic coiling up space, as predicted from theoretical investigations.

B. Static foundation effect on elastic coiling-up-space metamaterial

Unlike the acoustic coiling up space, the longitudinal band structure of the proposed metamaterial does not start at a zero frequency because the metamaterial does not strictly obey the isocurvature path condition. As explained

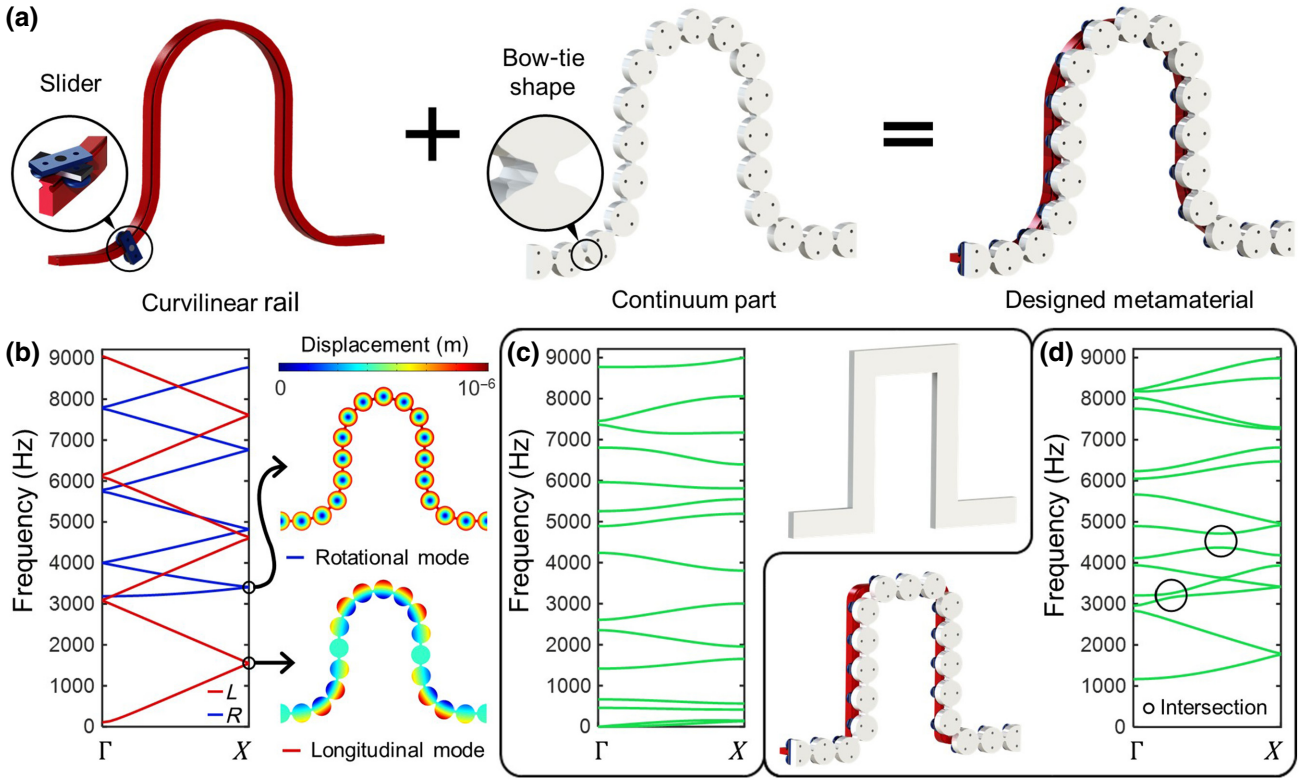

FIG. 4. (a) Design of elastic coiling-up-space metamaterial, (b) corresponding band structure and mode shapes. The red and blue lines indicate longitudinal and rotational branches, respectively. Design and corresponding band structure for (c) metamaterial that disobeys both specific conditions, (d) metamaterial that satisfies the fluidlike connection, but disobeys the isocurvature path. The green line indicates the mode-coupled branch.

earlier, a full isocurvature path forms a closed circular loop so that waves cannot enter or escape the elastic coiling up space. Therefore, the elastic coiling-up-space metamaterial is designed to have several singular points where the sign of the curvature changes. As shown in Fig. 5(c), there are six singular points in the metamaterial design. However, these singular points violate the isocurvature path condition. Thus, the inertial forces are required to change the direction of the displacement field at the singular points. Hence, where singular points exist, the so-called static foundation effect occurs in which the band structure has a nonzero starting frequency because the inertial force cannot exist at a zero frequency. As shown in Fig. 5(b), the elastic coiling-up-space metamaterial also has several singular points so that the band gap occurs at zero frequency, although it is almost negligible. By analyzing the mode shape at the point where the longitudinal band structure starts, it is clearly observed that the stresses are

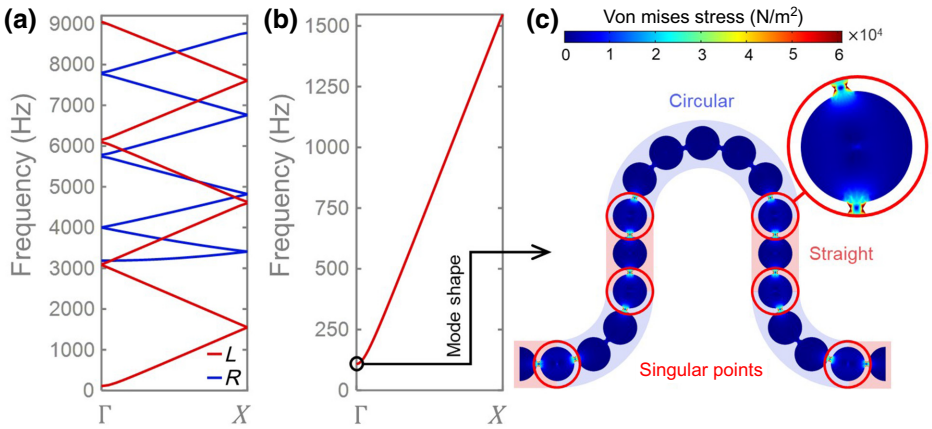

FIG. 5. (a) Band structure of elastic coiling-up-space metamaterial (the red and blue lines indicate longitudinal and rotational branches, respectively), (b) enlarged plot of band structure near zero frequency, (c) mode shape at the point at which the band structure starts.

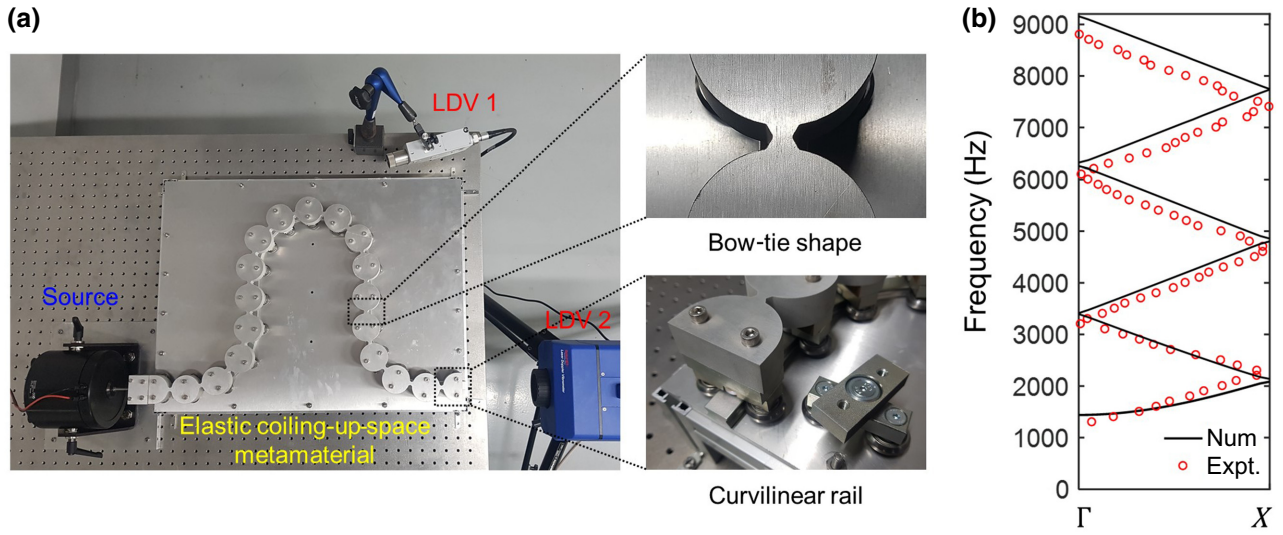

FIG. 6. (a) Experimental setup. (b) Numerically and experimentally obtained band structure of elastic coiling-up-space metamaterial. Herein, only the real-valued wave numbers are considered.

concentrated at the singular points at which the isocurvature is broken, as shown in Fig. 5(c). In summary, an elastic coiling-up-space metamaterial is inevitably designed to have several singular points so that the static foundation effect occurs, but its effect is negligibly small.

It is noteworthy that the rotational motion, plotted as the blue line in Fig. 5(a), also has the quasistatic band gap. This is also due to the static foundation effect, but its origin is somewhat different from the longitudinal motion's quasistatic band gap. The longitudinal wave's quasistatic band gap is due to the singular points, while the rotational motion's quasistatic band gap is due to the isocurvature path condition. To explain this, please note that the longitudinal motion is related to the motion on the slide, while the rotational motion is related to the motion perpendicular to the slide. Since the isocurvature path condition restricts each mass such that it can move only on the slide, if any excitation tries to provide motion perpendicular to the slide (related to the rotational motion), this condition suppresses it. Thus, there should be sufficient inertia to overcome this suppression to form propagating waves. At low frequencies, the inertia is very small so that propagating waves cannot be formed, resulting in the band gap below 3000 Hz.

IV. EXPERIMENTS

Finally, the proposed metamaterial is fabricated to experimentally validate our idea. First, the continuum part is fabricated by water-jet cutting with an aluminum plate of thickness 20 mm. After fabrication, the continuum part is placed on the curvilinear rail and slider (ROLLON CVRH01 and CCT08). Figure 6(a) shows a photograph of the experimental setup. The rail is fixed on the vibration table to avoid the effects of undesired external vibrations. The shaker, used as a source of longitudinal waves, is combined with metamaterials, and two laser Doppler vibrometers (LDVs) are used for measurements. The source signal for the experiment is generated with the use of a function generator, amplified by a power amplifier, and then sent to the shaker. For the input signal, sinusoidal wave packets of 10 wavelengths are used. The transmitted wave is measured simultaneously with the two LDVs placed at the center and at the end of the metamaterial. After the measurements, the effective phase velocity is calculated by the time difference between the peaks of the transmitted wave packets measured from two points. As a result, the band structure is experimentally obtained by calculating the wave number for each frequency using the calculated effective phase velocity. Note that since a single unit cell is used, it is impossible to evaluate band structure at high frequencies where the effect of periodicity becomes dominant. However, in the current research, we are focusing on the low-frequency regime where the effects of various wave dynamics are not significant, including periodicity, local resonance, etc. (please see the detailed information in Appendix C). Previous studies on acoustic and electromagnetic coiling up space have already shown that the coiling up space at low frequencies is governed by its own labyrinthine structure, not by periodicity, so a single unit is sufficient to achieve experimental data [2]. The band structure of the elastic coiling-up-space metamaterial obtained experimentally is shown in Fig. 6(b).

For comparison, the band structure of the fabricated metamaterial is numerically calculated. Although we do our best to reduce any undesired friction, friction exists that cannot be ignored in the experiments. Therefore, a numerical simulation should also consider the effect of

friction. Hence, we experimentally measure the amount of frictional force. Subsequently, the band structure is numerically calculated according to the frictional force condition. According to classical vibration theory, friction does not alter the phase; hence, the band structure is not highly affected [23]. However, it acts as a static foundation, which provides an additional band gap from zero frequency.

Figure 6(b) plots numerically and experimentally the measured band structures. Good agreement can be observed between the two results. At extremely low frequencies (around zero frequency), both numerical and experimental results show band gaps. It should be noted that in Fig. 6(b), only data above 1300 Hz are plotted because at frequencies lower than 1300 Hz, wave decay is observed so that the frequency range is obviously a bandgap range. As mentioned earlier, this is attributed to the unavoidable friction effect acting as the static foundation. However, except for the quasistatic band gap, there are no significant band gaps in the experimental results. Additionally, for the frequencies around the intersection points of the numerically calculated branches, no band gap is experimentally measured, showing that no mode coupling occurs in experiments. These experimental results strongly validate the fact that band folding without significant band gaps and mode coupling are observed experimentally. Thus, we conclude that the elastic coiling up space of the proposed metamaterial is validated experimentally.

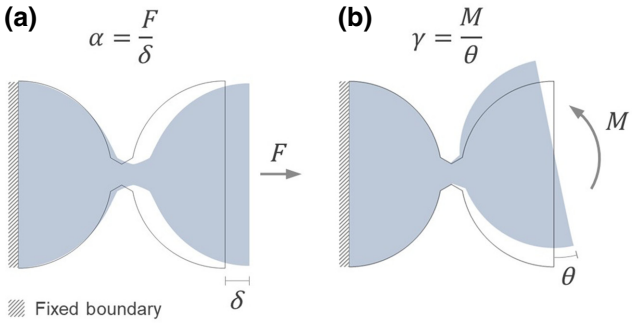

FIG. 7. Measurement methods of (a) translational spring coefficient, and (b) rotational spring coefficient.

V. CONCLUSIONS

In this study, we demonstrate a method to enable and realize elastic coiling up space. Owing to the tensorial nature of elasticity, elastic coiling up space has been considered unfeasible, unlike the acoustic case where waves are governed by the scalar field. From the theoretical approach, however, we show that elastic coiling up space is possible with two specific conditions, namely, the fluidlike connection condition and the isocurvature path condition. Based on these specific conditions, we design an elastic metamaterial for an elastic coiling up space. Numerical and experimental investigations of the designed metamaterial show that elastic coiling up space is indeed possible under specific conditions. Considering the significant advances enabled by acoustic coiling up space, our idea of achieving elastic coiling up space is expected to suggest a powerful method to design elastic metamaterials and contribute to advances in elastic metasurfaces. For instance, by combining our research with various techniques of impedance matching (by redesigning the unit or adding additional structure [24]), our elastic coiling up space could suggest a convenient way to provide phase shifts for broad frequency ranges, which is one of the most important characteristics in elastic metasurfaces. In particular, considering that low-frequency broadband wave control is still a great challenge and an attractive research topic in elastic metasurfaces [25], the advantages of the elastic coiling up space that can make broadband wave control possible from near-zero frequency become even more apparent. Accordingly, our research can provide various metasurface designs at broad frequency ranges, unlike almost all elastic metasurfaces based on resonance. In addition, considering that the wavelength inside the coiling-up-space metamaterial is extremely small, our coiling-up-space metamaterial can provide extremely small metamaterial devices. This would be especially important in low-frequency applications, such as vibration absorption or seismic blocking, which are currently one of the most challenging issues in metamaterial applications.

ACKNOWLEDGMENTS

This work was supported by the Center for Advanced Meta-Materials (CAMM) funded by the Ministry of Science, ICT and Future Planning as Global Frontier Project (CAMM-2014M3A6B3063711), by the National Research Foundation of Korea (NRF) grants funded by the Korean government (Grants No. 2021R1A4A1033224,

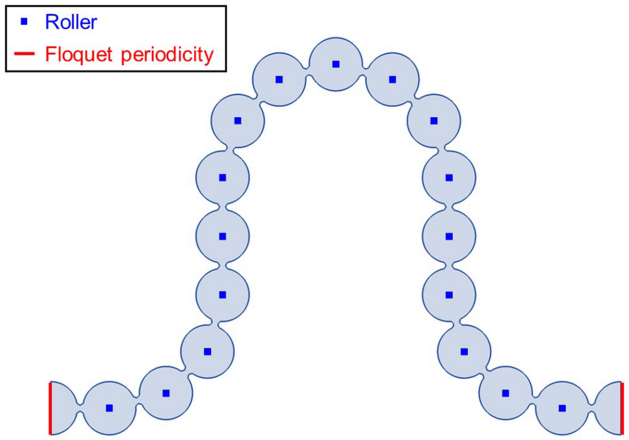

FIG. 8. Numerical settings of eigenfrequency analysis to obtain band structure.

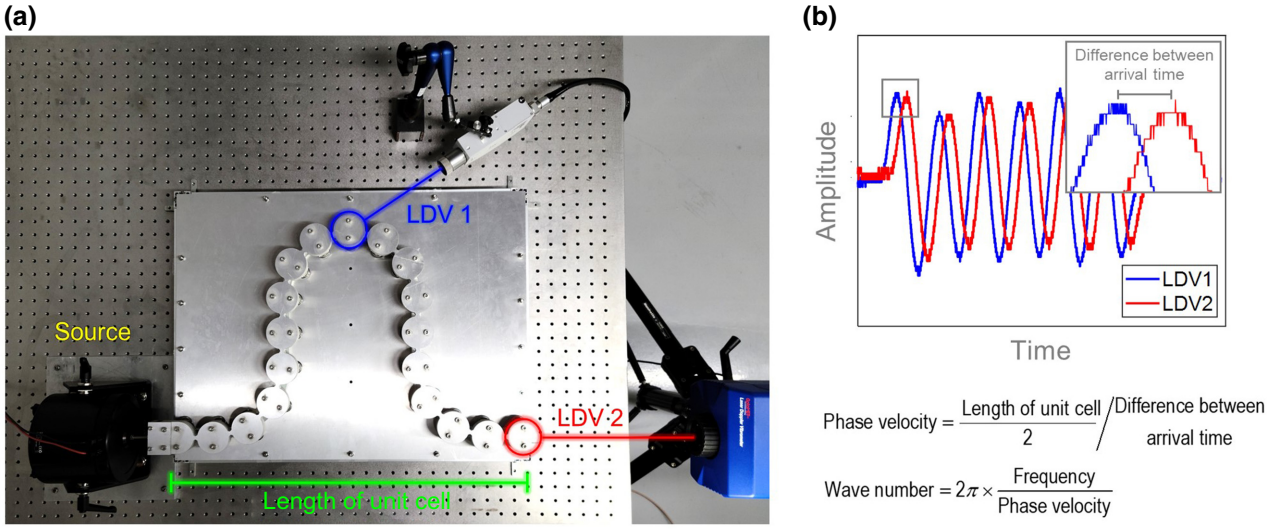

FIG. 9. (a) Experimental setup. (b) Experimental methods to obtain band structure.

No. 2020R1A2C4002383, and No. 2020M3F6A108180512), by the National Research Council of Science & Technology (NST) grant by the Korean government (MSIP; Grant No. CAP-17-04-KRISS).

APPENDIX A: MEASUREMENT OF THE SPRING CONSTANTS

To validate whether the rotational stiffness of the designed elastic coiling-up-space metamaterial is sufficiently small compared to the longitudinal stiffness, the translational and rotational spring coefficients are measured via numerical simulation. Note that the shear spring coefficient is excluded from the measurement because there is no shear motion in elastic coiling-up-space metamaterials due to the curvilinear rail. The spring coefficients are calculated as follows. First, proper force (for instance, longitudinal force is applied to measure the translational stiffness, while the moment is applied to measure the rotational spring coefficient) is applied to the internal structure of the elastic coiling-up-space metamaterial. After that, the proper displacement (longitudinal displacement for the translational stiffness case, and the rotational angle for the rotational stiffness) is measured so that the corresponding spring coefficient is derived from the relationship between displacement and force, as shown in Figs. 7(a) and 7(b).

The calculated translational spring coefficient is 2.18×10^{10} N/m, and the rotational spring coefficient is 2.23×10^{5} Nm/rad. These values validate that the rotational spring coefficient is negligible compared to the translational spring coefficient, i.e., the elastic coiling-up-space metamaterial, designed based on the bow-tie shape, has a very small rotational stiffness compared with its longitudinal stiffness.

APPENDIX B: NUMERICAL SETTINGS AND EXPERIMENTAL METHODS

Here, numerical simulation settings and detailed experimental methods are described. In the numerical simulation, the commercial program COMSOL Multiphysics is used. The band structure of the elastic coiling-up-space metamaterial is calculated by eigenfrequency analysis with the Floquet periodicity. Numerical simulation settings are shown in Fig. 8. To model the periodically arranged unit cells, Floquet periodicity is imposed at both ends of the elastic coiling-up-space metamaterial. Additionally, roller conditions are applied for the center point of each mass to mimic the sliders and the curvilinear rail. Here, the roller condition is applied to a point rather than a line

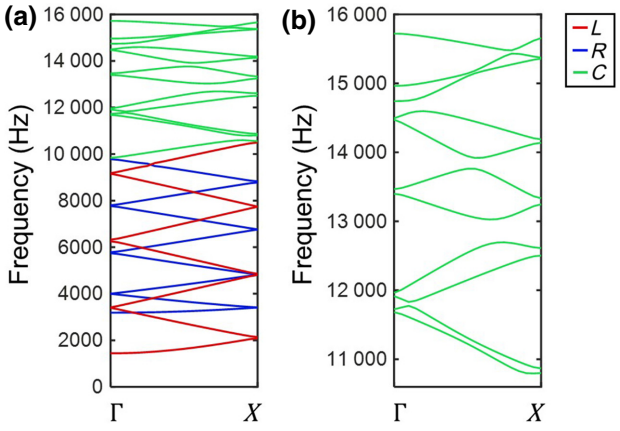

FIG. 10. (a) Band structure of elastic coiling-up-space metamaterial including high-frequency regime (the red, blue, and green lines indicate the longitudinal, rotational, and mode-coupled branches, respectively), (b) enlarged plot of band structure in the high-frequency regime.

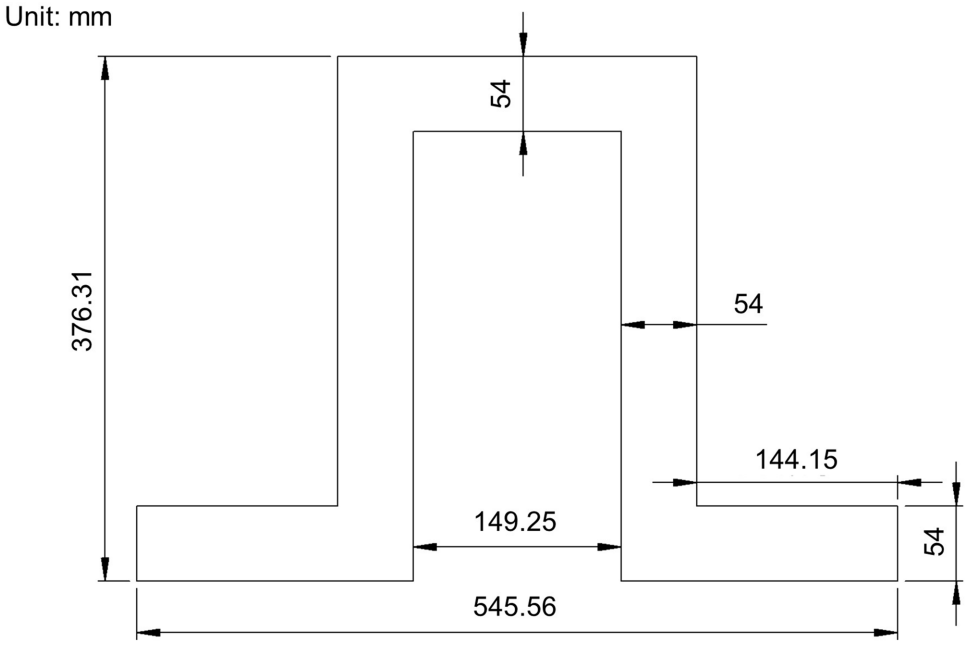

FIG. 11. Detailed geometries and sizes of metamaterial with simple continuum structure that disobeys both the fluidlike connection and isocurvature path conditions.

since all masses must be able to freely rotate while moving along the curvilinear path, as like masses on the sliders of curvilinear rail. Aluminum's material properties, density $\rho = 2700$ (kg/m^3), Young's modulus $E = 70$ (GPa), and Poisson's ratio $\upsilon = 0.32$, are applied.

The experimental setup to obtain the band structure of the elastic coiling-up-space metamaterial is shown in Fig. 9(a). The overall experimental methods are as follows. First, a longitudinal wave packet, which is a sinusoidal packet consisting of 10 periods, is generated at the left-hand end by the shaker. The propagation of wave packets is measured by two laser Doppler vibrometers, LDV 1 and LDV 2, placed at the middle and end of the unit cell. From the data measured at LDV 1 and LDV 2, the arrival times for the first peak of the wave packets are obtained, respectively. Here, the difference between arrival times is the time required for the first peak of the wave packets to propagate the distance between the two points. Since the size of the unit cell is known, the effective phase velocity can be calculated by dividing the distance between the two points by the arrival times. After measuring the effective phase velocity, the wave number is calculated from the relation between frequency and phase velocity ($\omega = kc$, where ω is the angular frequency, k is the wave number, and c is phase velocity). As a result, the wave number for each frequency, i.e., the band structure, is obtained experimentally.

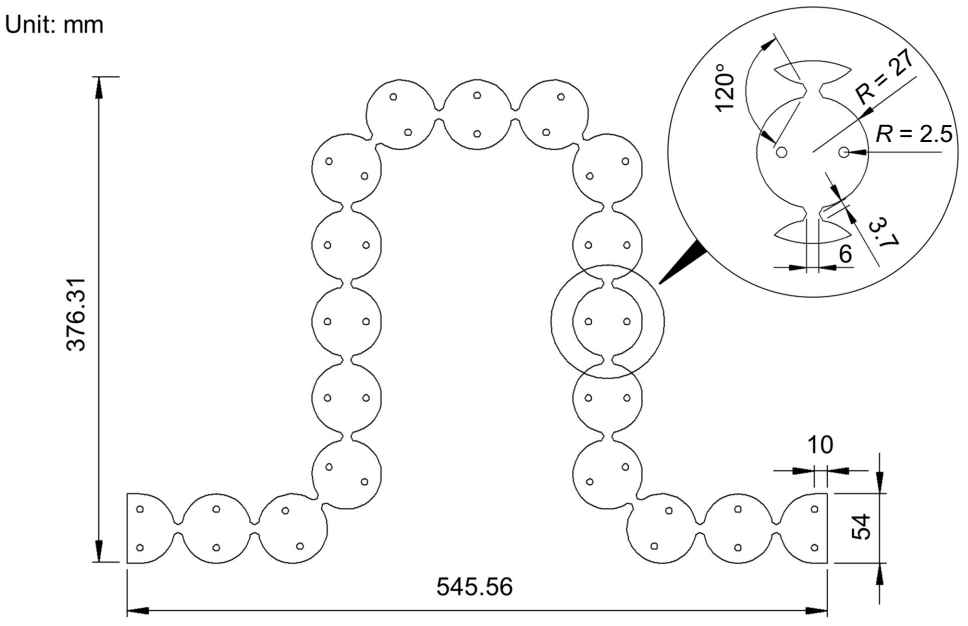

FIG. 12. Detailed geometries and sizes of metamaterial that satisfies the fluidlike connection but disobeys the isocurvature path condition.

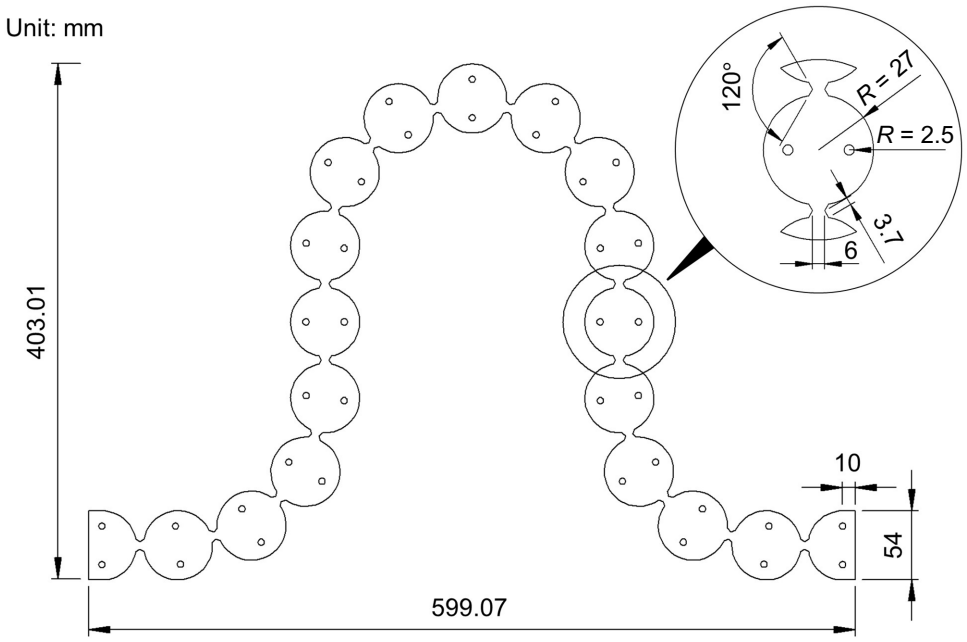

FIG. 13. Detailed geometries and sizes of elastic coiling-up-space metamaterial that satisfies both specific conditions.

APPENDIX C: EFFECTS OF VARIOUS WAVE DYNAMICS IN THE HIGH-FREQUENCY REGIME

In our work, we used the rigid-body based approach to figure out two main conditions, fluidlike connection and isocurvature path, for elastic coiling up space. However, since the approach is based on the static insight, it works for the low-frequency regime only. At low frequencies, two main conditions strongly suppress the elastic nature so that elastic coiling up space is achievable. However, in the high-frequency regime, the effects of the elastic tensorial nature become strong and cannot be ignored. For instance, undesired wave phenomena inevitably occur, such as Bragg scattering due to the periodicity and local resonance of the internal structure. In addition, mode coupling, which is restricted by the specific conditions of fluidlike connection and isocurvature path, also occurs in

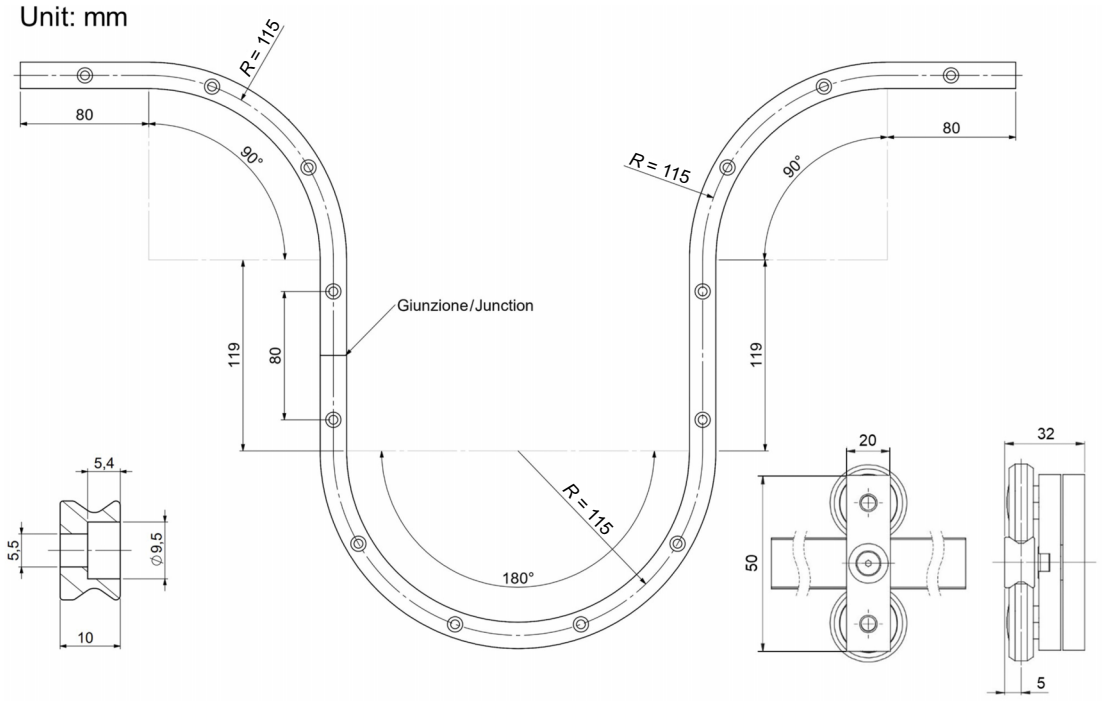

FIG. 14. Detailed geometries and sizes of curvilinear rail and slider.

the high-frequency regime. Thus, our research focuses on the low-frequency regime only.

To further clarify this point, the band structure of the elastic coiling-up-space metamaterial including the high-frequency regime is shown in Fig. 10. As shown in Fig. 10, below 10 000 Hz, undesired wave phenomena, such as Bragg scattering, local resonance, and mode coupling, do not occur in the band structure. However, above 10 000 Hz, it can be seen that various band gaps exist, originating from the Bragg scattering and mode coupling. Since the two conditions are derived from the static case, they work well for low frequencies so that the Bragg scattering and mode coupling is well suppressed. However, at high frequencies, these conditions do not work well so the elastic tensorial nature becomes dominant again. This is why various band gaps and mode coupling become active again at the high frequencies.

Note that the wave physics at such high frequencies cannot be described by the conventional mass-spring system shown in this work. Unlike at low frequencies, it is hard to define which structure acts as spring or mass. Nevertheless, as shown in Fig. 10, our research is valid for low frequencies. The way to achieve elastic coiling up space at high frequencies could be a challenging topic for further research.

APPENDIX D: DETAILED GEOMETRIES AND SIZES

The detailed geometries and sizes of the elastic coiling-up-space metamaterial and comparison groups in the main article are shown in Figs. 11–13. Additionally, detailed geometries and sizes of curvilinear rails and sliders for the elastic coiling-up-space metamaterial are also shown in Fig. 14. In Figs. 12–14, R denotes the radius.

[1] Z. Liang and J. Li, Extreme Acoustic Metamaterial by Coiling up Space, Phys. Rev. Lett. **108**, 114301 (2012).

[2] Y. Xie, B.-I. Popa, L. Zigoneanu, and S. A. Cummer, Measurement of a Broadband Negative Index With Space-Coiling Acoustic Metamaterials, Phys. Rev. Lett. **110**, 175501 (2013).

[3] S. K. Maurya, A. Pandey, S. Shukla, and S. Saxena, Double negativity in 3D space coiling metamaterials, Sci. Rep. **6**, 33683 (2016).

[4] Y. Li, B. Liang, X. Tao, X.-F. Zhu, X.-Y. Zou, and J.-C. Cheng, Acoustic focusing by coiling up space, Appl. Phys. Lett. **101**, 233508 (2012).

[5] Y. Li, G. K. Yu, B. Liang, X. Y. Zou, G. Y. Li, S. Cheng, and J. C. Cheng, Three-dimensional ultrathin planar lenses by acoustic metamaterials, Sci. Rep. **4**, 6830 (2014).

[6] G. Y. Song, B. Huang, H. Y. Dong, Q. Cheng, and T. J. Cui, Broadband focusing acoustic lens based on fractal metamaterials, Sci. Rep. **6**, 35929 (2016).

[7] S. Qi, Y. Li, and B. Assouar, Acoustic Focusing and Energy Confinement Based on Multilateral Metasurfaces, Phys. Rev. Appl. **7**, 054006 (2017).

[8] S. Qi and B. Assouar, Acoustic energy harvesting based on multilateral metasurfaces, Appl. Phys. Lett. **111**, 243506 (2017).

[9] Y. Li, B. Liang, X. Y. Zou, and J. C. Cheng, Extraordinary acoustic transmission through ultrathin acoustic metamaterials by coiling up space, Appl. Phys. Lett. **103**, 063509 (2013).

[10] H. Ryoo and W. Jeon, Perfect sound absorption of ultra-thin metasurface based on hybrid resonance and space-coiling, Appl. Phys. Lett. **113**, 121903 (2018).

[11] Y. Wang, H. Zhao, H. Yang, J. Zhong, D. Zhao, Z. Lu, and J. Wen, A tunable sound-absorbing metamaterial based on coiled-up space, J. Appl. Phys. **123**, 185109 (2018).

[12] F. Wu, Y. Xiao, D. L. Yu, H. G. Zhao, Y. Wang, and J. H. Wen, Low-frequency sound absorption of hybrid absorber based on micro-perforated panel and coiled-up channels, Appl. Phys. Lett. **114**, 151901 (2019).

[13] K. Donda, Y. Zhu, S.-W. Fan, L. Cao, Y. Li, and B. Assouar, Extreme low-frequency ultrathin acoustic absorbing metasurface, Appl. Phys. Lett. **115**, 173506 (2019).

[14] X. F. Man, T. T. Liu, B. Z. Xia, Z. Luo, and L. X. Xie, Space-coiling fractal metamaterial with multi-bandgaps on subwavelength scale, J. Sound Vib. **423**, 322 (2018).

[15] G. J. Jeon and J. H. Oh, Nonlinear acoustic metamaterial for efficient frequency down-conversion, Phys. Rev. E **103**, 012212 (2021).

[16] X. Ni, Y. Wu, Z. G. Chen, L. Y. Zheng, Y. L. Xu, P. Nayar, X. P. Liu, M. H. Lu, and Y. F. Chen, Acoustic rainbow trapping by coiling up space, Sci. Rep. **4**, 7038 (2014).

[17] R. Al Jahdali and Y. Wu, High transmission acoustic focusing by impedance-matched acoustic meta-surfaces, Appl. Phys. Lett. **108**, 031902 (2016).

[18] Z. Liang, T. Feng, S. Lok, F. Liu, K. B. Ng, C. H. Chan, J. Wang, S. Han, S. Lee, and J. Li, Space-coiling metamaterials with double negativity and conical dispersion, Sci. Rep. **3**, 1614 (2013).

[19] S. D'Agostino, F. Emma, and C. Paolini, Accurate analysis of helix slow-wave structures, IEEE Trans. Electron Devices **45**, 1605 (1998).

[20] G. Ma, C. Fu, G. Wang, P. del Hougne, J. Christensen, Y. Lai, and P. Sheng, Polarization bandgaps and fluid-like elasticity in fully solid elastic metamaterials, Nat. Commun. **7**, 13536 (2016).

[21] J. H. Oh and B. Assouar, Quasi-static stop band with flexural metamaterial having zero rotational stiffness, Sci. Rep. **6**, 33410 (2016).

[22] H. W. Park, H. M. Seung, M. Kim, W. Choi, and J. H. Oh, Continuum Flexural Metamaterial for Broadband low-Frequency Band Gap, Phys. Rev. Appl. **15**, 024008 (2021).

[23] D. J. Inman, *Engineering Vibration* (Prentice-Hall, Englewood Cliffs, NJ, 1996).

[24] T. Gomez and F. Montero, Bridging the gap of impedance mismatch between air and solid materials, IEEE Ultrason. Symp. **2**, 1069 (2000).

[25] L. Cao, Z. Yang, Y. Xu, S. W. Fan, Y. Zhu, Z. Chen, Y. Li, and B. Assouar, Flexural wave absorption by lossy gradient elastic metasurface, J. Mech. Phys. Solids **143**, 104052 (2020).